Annales Geophysicae (2004) 22: 1–8
SRef-ID: 1432-0576/ag/2004-22-1

Annales Geophysicae

Characterization of VHF radar observations associated with equatorial Spread F by narrow-band optical measurements

R. Sekar[1], **D. Chakrabarty**[1], **R. Narayanan**[1], **S. Sripathi**[2], **A. K. Patra**[2], **and K. S. V. Subbarao**[3]

[1]Physical Research Laboratory, Ahmedabad, India
[2]National MST Radar Facility, Gadanki, Tirupati, India
[3]Space Physics Laboratory, Vikram Sarabhai Space Center, Thiruvananthapuram, India

Received: 21 October 2003 – Revised: 28 May 2004 – Accepted: 8 June 2004 – Published:

Part of Special Issue "ELLA"

Abstract. The VHF radars have been extensively used to investigate the structures and dynamics of equatorial Spread F (ESF) irregularities. However, unambiguous identification of the nature of the structures in terms of plasma depletion or enhancement requires another technique, as the return echo measured by VHF radar is proportional to the square of the electron density fluctuations. In order to address this issue, co-ordinated radar backscatter and thermospheric airglow intensity measurements were carried out during March 2003 from the MST radar site at Gadanki. Temporal variations of 630.0-nm and 777.4-nm emission intensities reveal small-scale ("micro") and large-scale ("macro") variations during the period of observation. The micro variations are absent on non-ESF nights while the macro variations are present on both ESF and non-ESF nights. In addition to the well-known anti-correlation between the base height of the F-region and the nocturnal variation of thermospheric airglow intensities, the variation of the base height of the F-layer, on occasion, is found to manifest as a bottomside wave-like structure, as seen by VHF radar on an ESF night. The micro variations in the airglow intensities are associated with large-scale irregular plasma structures and found to be in correspondence with the "plume" structures obtained by VHF radar. In addition to the commonly observed depletions with upward movement, the observation unequivocally reveals the presence of plasma enhancements which move downwards. The observation of enhancement in 777.4-nm airglow intensity, which is characterized as plasma enhancement, provides an experimental verification of the earlier prediction based on numerical modeling studies.

Key words. Airglow and aurora; equatorial ionosphere; ionspheric irregularities

Correspondence to: R. Sekar
(rsekar@prl.ernet.in)

1 Introduction

The structures and dynamics of equatorial Spread F (ESF) irregularities have been investigated with VHF backscatter radar which is one of the powerful tools to simultaneously observe the bottomside and topside ionospheric irregularities. Many observations from various longitudinal sectors (Tsunoda, 1980; Patra et al., 1995) have been reported ever since the first backscatter radar observation was reported by Woodman and La Hoz (1976). In order to understand different aspects of ESF, a number of co-ordinated measurements have been carried out by different workers (Szuszezewicz et al., 1980; Kelley et al., 1986; Raghavarao et al., 1987; Sridharan et al., 1997). Plasma irregularities associated with equatorial Spread F manifest themselves in a variety of forms on VHF radar maps ranging from rising plumes and multiple plumes to ESF structures confined to the bottomside of the ionosphere. A few meter scale size irregularities are generally responsible for the back scatter echoes recorded by the VHF radar. The causative mechanism for the ESF irregularities in the scale sizes of 1–10 m is not yet comprehensively understood (Huba and Ossakow, 1979). However, co-ordinated measurements (Szuszezewicz et al., 1980; Kelley et al., 1986) have revealed that the plume structures as observed by the VHF radar are the manifestations of large-scale plasma bubbles generated by the action of collisional Rayleigh-Taylor (CRT) instability (Haerendel, 1974) and associated nonlinear processes (Ossakow, 1981; Sekar et al., 1994). The multiple plume structures are generated by CRT instability seeded by spatially varying electric fields associated with gravity waves (Huang and Kelley, 1996). The confinement of ESF structures to the bottomside of the ionosphere was shown (Sekar and Kelley, 1998) to be due to the combined action of vertical shear in zonal plasma drift and westward electric field associated with a particular temporal pattern of the zonal electric field. Thus, the VHF radar echoes have been used to interpret the physical processes as-

sociated with the large-scale equatorial Spread F structures. The Doppler velocities inside some of the structures are predominantly upward which are generally associated with a plasma bubble. However, downward velocities inside the structures are also not uncommon (Patra et al., 1997; Rao et al., 1997; Laakso et al., 1994). The structures observed by VHF radar moving with downward drift could be associated with plasma enhancements under certain conditions. On the other hand, the "fossil" bubble (plasma depletion in non-evolutionary phase), under the action of westward ambient electric field, can also move downward. Thus, the presence of downward movement in the RTV (Range-Time-Velocity) map need not unequivocally indicate the presence of enhancement structures. As the radar technique alone is inadequate to identify the nature of the structures, simultaneous airglow measurements have also been carried out to characterize the VHF radar observations.

Airglow photometry in multiple wavelengths can serve as a potentially complementary technique to address the above issue. The structures in ESF, particularly those with large-scale sizes, have been studied using scanning optical photometers (Takahashi et al., 1989; Sipler et al., 1981) and all-sky imagers (Weber et al., 1978; Sahai et al., 1994; Mendillo et al., 1997; Sinha et al., 1996). Depletions and enhancements in airglow intensities during ESF events (Mendillo et al., 1985; Sinha et al., 1996) have been recorded by imagers. Thermospheric airglow emissions like 630.0-nm from ∼250–300 km altitude region and 777.4-nm from the F-region peak altitude have generally been used as tracers to record the modulations in the F-region ionization. It is known that the 630.0-nm emission line intensity during nighttime is proportional to the electron density, as the emission process is an outcome of dissociative recombination of O_2^+ with the ambient electron. Similarly, the 777.4-nm emission intensity due to the radiative recombination process of O^+ is proportional to the square of the electron densities. However, the temporal variation in 777.4-nm emission intensity is directly proportional to the product of electron density and its variation. In view of these aspects, both these thermospheric emission line intensities are used to infer the modulations in the F-region ionosphere. The modulations in the temporal variation of nocturnal airglow intensities have been found to be associated with the variations in the F-layer heights (Barbier, 1959), with the well-known equatorial reverse plasma fountain (Kulkarni and Rao, 1972; Sridharan et al., 1993; Sekar et al., 1993), with the meridional wind reversal associated with midnight temperature anomaly (Herrero and Meriwether, 1980) and plasma depletions (Sipler et al., 1981). Most of the earlier studies have been carried out using photometers having a broad spectral range (band width ranging from 0.6-nm to a few nm) and as a consequence, without the requirement of stringent temperature tuning of the interference filters used. On the other hand, the airglow imagers which have been usually deployed for ESF investigations are devices aimed at having large spatial coverage (large field of view) and hence filters with large bandwidth are used. A narrow band (∼0.3-nm) photometer, along with the ALTAIR radar (Sipler et al., 1981), was operated to obtain all-sky map of airglow intensities which revealed airglow depletions. Although the plasma drift velocities obtained by the photometer were compared with the line-of-sight neutral wind velocities measured by a collocated airglow spectrometer, the variations in the airglow intensity were not compared with the ESF structures obtained by the radar.

In order to unravel the association of the variations in the airglow intensity with the ESF structures revealed by VHF radars, a co-ordinated campaign was conducted at Gadanki (13.5° N, 79.2° E, dip lat. 6.3° N) by simultaneously operating the MST radar and a narrow pass-band photometer. Co-ordinated observations are available for a few nights. In this communication, we present the range-time-intensity (RTI) and range-time-velocity (RTV) maps obtained by the VHF radar with the emission intensities from the thermospheric airglow lines of 630.0-nm and 777.4-nm on an ESF and a non-ESF night.

2 Experimental details

The mesosphere-stratosphere-troposphere (MST) radar at Gadanki is a high power coherent pulsed radar. It operates at 53 MHz and can attain a maximum power aperture product of 3×10^{10} Wm^2. The radar system consists of (i) a total of 1024 three element Yagi antennas arranged in two orthogonal sets, (ii) 32 high power transmitters, (iii) 32 units of transmit-receive duplexes, and (iv) a phase coherent receiver. A detailed description of various subsystems (Rao et al., 1995) and the observation of equatorial Spread F irregularities using this radar for the first time (Patra et al., 1995) were reported earlier. In order to obtain echoes from field aligned ESF irregularities, the radar beam was oriented 14.8° N from zenith which makes the beam transverse to the Earth's magnetic field at F-region altitudes.

A multi-wavelength scanning nighttime photometer has recently been developed at the Physical Research Laboratory to study the airglow emission intensities from the thermosphere and mesosphere. This photometer comprises of three sections, namely the front-end optics, the filter section and a detector section. A front end optics, containing a camera and collimating lenses, along with a field stop (field-of-view of ∼ 3° which is similar to the VHF radar beamwidth), is used to collimate the beam. The filter section is kept in the collimated portion of the beam. A rotating platform consisting of four filter assemblies is arranged in such a way that one of the filter assemblies becomes optically aligned with the front end optics and the detector attached beneath the filter section. Narrow band (band width ∼0.3-nm) temperature tuned interference filters are used in these filter assemblies. A typical filter assembly consists of a brass chamber enclosed in thermally insulated housing that provides isolation from the environment. The temperature of the brass chamber is controlled using a bi-polar temperature controller which employs Peltier elements and AD-590 temperature sensors (accuracy of ∼ 0.1°C). Finally, the filtered beam is focussed

on the cathode of a photomultiplier tube (S-20; EMI 9863) housed in a temperature controller unit provided by EMI. A reasonably fast scanning mirror assembly was attached on top of the front end optics. The rotation of the filter platform and the mirror scanning are controlled by a computer. However, in the present communication, results obtained from vertical direction only are discussed.

In addition to the VHF radar and optical measurements, information on the ionospheric height parameter h'F are obtained from a digital ionosonde (KEL make, Model IPS42) which is being systematically operated from SHAR, a station 100 km east of Gadanki. The temporal resolution of the ionograms obtained for the present campaign is only 15 minutes.

3 Results

Figure 1 depicts composite results obtained from both VHF radar and airglow photometer on 25 March 2003 when ESF was present. The horizontal axis corresponds to time in IST (Indian Standard Time, IST=Universal Time, UT+5.5 h) which is common for all the subplots. The range-time-intensity (RTI) and range-time-velocity (RTV) of the radar echoes are plotted in subplots (A and B). The colour codes in them correspond to the intensity of return echoes in (A) and line-of-sight Doppler velocities in (B). The vertical columnar intensities of 630.0-nm and 777.4-nm airglow emissions are depicted in (C) and (D) subplots of Fig. 1. The RTI map in Fig. 1A consists of wave-like bottomside structures and vertically rising and/or slanted plume structures in the height region above 350 km. The velocities in the bottomside structures are predominantly downward except during 20.25 to 20.5 and 21.75 to 22.25 IST. The velocities inside plume structures are upward in certain regions and downward in other regions. Downward velocities of the order of 50 m/s are also seen. The temporal variation of the 630.0-nm airglow intensities in Figure 1C comprises of a monotonic decrease during the initial phase along with macro and micro variations in the later phase. The macro variations are marked at the nodal points by alphanumerical letters L1 to L7. It is to be noted that any variation in the airglow intensity which spans in time $\leq$15 min and in amplitude $\sim$2–3 times more than the statistical noise level (square root of the count level) is considered to be a "micro" variation. They are marked at the regions of mutual correspondence by the tips of the pointers emanating from the symbol boxes denoted by "S". These boxes are placed suitably to avoid cluttering and to prevent them obscuring the structures shown by the radar map. In Fig. 1C, the micro variations are denoted by S4 to S7. Note that the symbols corresponding to micro variations are marked in the RTV maps instead of the RTI maps for the purpose of clarity. The altitude variation of the base height of the F-region (h'F) obtained from the ionograms over SHAR, a station 100 km east of the radar site is also plotted in Fig. 1C along with the temporal variation of the 630.0-nm intensity. The macro variations in the 777.4-nm airglow intensity in Fig. 1D are reasonably similar with those in the 630.0-nm intensity corresponding to Fig. 1C. In addition to them, micro variations are seen in between 20.5 to 20.75 IST, which are denoted by S1 to S3. Note that these micro variations are present only in 777.4-nm intensities corresponding to high altitude plume structures in Fig. 1A. The micro variations such as S4 and S6 are present in both the emission lines while the micro variation denoted by S7 is present only in 630.0-nm emission line.

Figure 2, consisting of similar subplots (2A-D), depicts the corresponding temporal variations on a night (27 March 2003) when ESF activity was not present. As expected, there is no VHF radar structure in the F-region, only some E-region structures. In subplots 2C and 2D micro variations above the statistical noise are not seen. However, macro variation in the airglow intensity corresponding to the F-region base height (h'F) variation is observed. The temporal variation of the F-region base height depicted in the subplot 2C is found to be in anti-correlation with the macro variation present in 630.0-nm intensity.

The 777.4-nm emission intensities on both nights are, in general, less intense compared to the 630.0-nm emission intensities as the radiative recombination rate responsible for 777.4-nm emission is orders of magnitude smaller than the dissociative recombination rate. Further, the quantum efficiency of the photomultiplier tube used in the present optical experiment is less in the wavelength regime of 777.4-nm compared to 630.0-nm. Thus, the statistical noises are higher in 777.4-nm emission intensities. In order to reduce the statistical noise in 777.4-nm intensity variation, the following procedure is adopted. The time series data obtained on 25 March 2003 were subjected to Fourier analysis and a low pass filter (frequencies more than 6 cycles/h are eliminated) was applied in the frequency domain and a reconstruction was made in the time domain. Figure 3 depicts the reconstructed data along with the original one. All the micro variations marked in Fig. 1 are clearly seen in the reconstructed data.

4 Discussion

The optical observations obtained on an equatorial Spread F night (25 March 2003) exhibit macro and micro intensity variations (see Fig. 1C–D). The nodal points indicating phase changes in the macro variations of 630.0-nm intensity are in anti-correlation (intensity maximum coincide with altitude minimum) with the phase changes in the observed bottomside wave- like structures on the RTI map depicted in Fig. 1a. As expected from the well-known Barbier type relation, the macro variations in the airglow intensities are found to be anti-correlated with the variation of the base height of F-region. However, the amplitudes of the large-scale structure in 630.0-nm variations are not proportional to the amplitude variation of F-region base height. This can be attributed to the additional role played by the F-region electron density to the 630.0-nm emission intensities as given by the Barbier relation (Barbier, 1959). Certain characteristic low-latitude

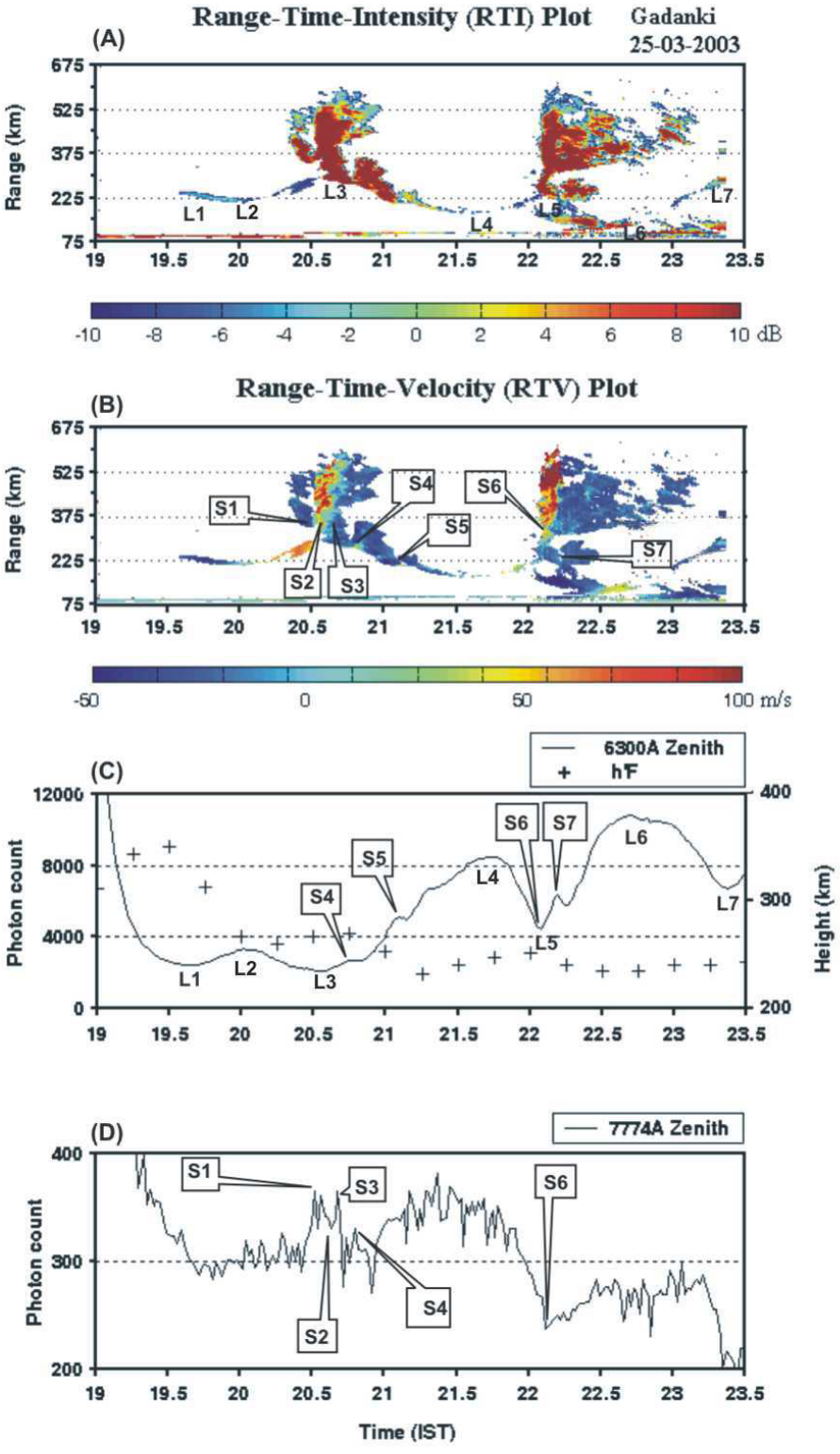

Fig. 1. Composite plots of temporal variations of (**A**) Range and Intensity (RTI), (**B**) Range and Velocity (RTV), (**C**) 630.0-nm airglow intensity (solid line) along with h'F (+) and (**D**) 777.4 nm airglow intensity on an equatorial Spread F night, 25 March 2003. The colour codes in (A) and (B) denote the intensity and the velocity respectively. L1 to L7 represent the nodal points of the macro variations in airglow intensity corresponding to the bottomside structures revealed by RTI map. S1 to S7 represent the region of mutual correspondence between the radar structures and the micro variations in the airglow intensity. Note that the variations denoted by S1 to S3 are only in 777.4-nm while the variation denoted by S7 is only in 630.0-nm. However, the variarions denoted by S4 to S6 are found in both the emission lines.

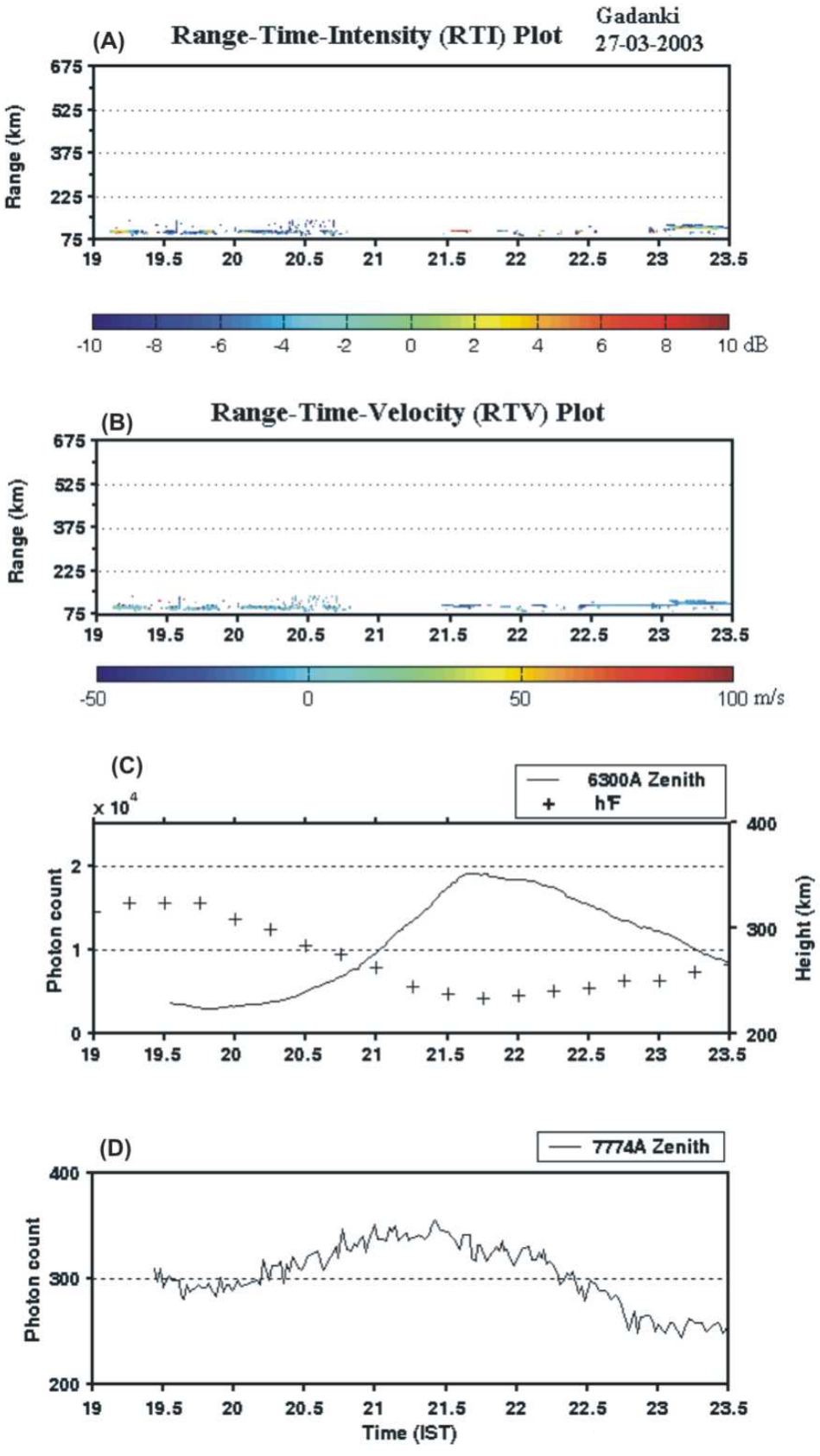

Fig. 2. Similar to Fig. 1 showing the absence of micro variations in the airglow intensity on a non-ESF night, 27 March 2003.

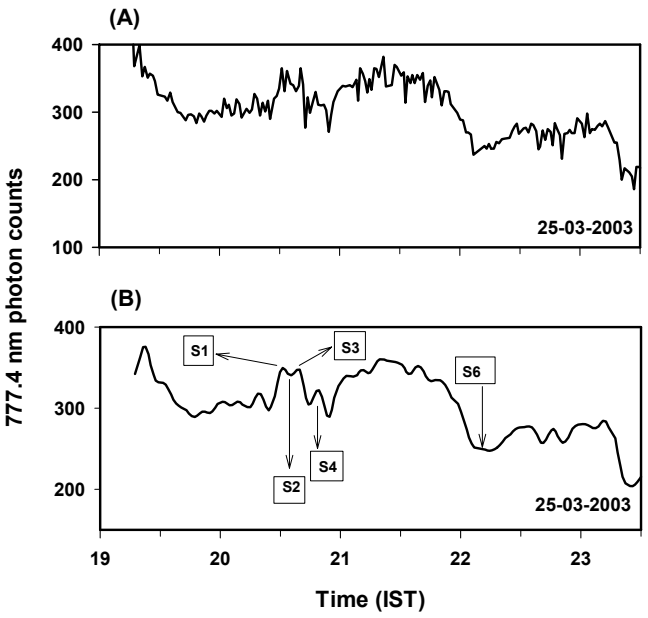

Fig. 3. (**A**) Nocturnal variation of 777.4-nm intensity on 25 March 2003 as observed by the photometer and (**B**) reconstructed variation after the removal of high frequency components in the frequency domain.

processes, like the reverse fountain effect and/or the midnight temperature anomaly, may also contribute to the above mentioned departure in amplitude. However, the similarities in the macro variations of both the line emissions (630.0-nm and 777.4-nm) suggest that these macro variations are mainly due to the altitude variations of the F-layer. As the macro variations in airglow intensity primarily depend on the base height variation of the F-region, they are also found on the nights when ESF is not observed (see Fig. 2). On certain equatorial Spread F nights, variations in the F-region base height manifest as a bottomside large scale wave-like structure, depending on the amplification by Rayleigh-Taylor instability mechanism of large-scale perturbation associated with the F-region layer movement.

The micro variations observed in 630.0-nm and 777.4-nm intensities are found to be in correspondence with the plume structures in RTI maps. Those plume structures, whose roots extend up to 250 to 300 km altitude region, such as S4 to S7, register their presence as micro variations in 630.0-nm intensity and those plume structures which spread over F-region peak altitude register their signatures only in 777.4-nm intensity. For example, the structures in the RTI maps corresponding to S1 to S3, have optical signatures only in 777.4-nm and not in 630.0-nm intensity. In addition to the micro variations (see S2 and S6) corresponding to plasma depleted structures, micro variations (see S1, S3 and S7) corresponding to plasma enhancement structures are also observed. Some of these micro variations (see S1 and S3) which represent plasma enhancement structure, extend well above 350 km with corresponding significant downward movement[1]. This is evidence for an enhancement which is seen well above 350 km in a buoyancy dominated region which cannot be controlled by ambient westward electric field alone. Further, micro variations are found to be absent on the night when ESF is not observed. Thus, the micro variations are essentially associated with plasma structures developed during ESF activity.

The upward moving depletions have been observed by other optical measurements involving imaging techniques (Mendillo et al., 1985; Sinha et al., 1996). The measurements of airglow enhancement flanking depletions were reported over Asian (Sinha et al., 1996) and South American (Mendillo et al., 1985) longitudes using imagers with wide band filters. Mendillo et al. (1985) compared their observation with the simulation studies using a long wavelength mode as seed perturbation. This study (Mendillo et al., 1985) revealed that the airglow depletions corresponding to ESF bubble structure were flanked by regions with relatively enhanced plasma concentration. However, in this investigation the variation of the background F-region of the ionsphere is not included. As discussed earlier, the background F-region movement can also manifest into macro variation in airglow intensity in the temporal domain. Therefore, using an imaging technique, which employs a wide band filter and wide angle coverage, it is difficult to differentiate whether those airglow structures (particularly in 630.0-nm) correspond to the F-region height variation or are due to plasma processes associated with ESF structures, especially when the observation site is close to the magnetic equator. With the help of such imaging technique, it is easier to identify the ESF structures which correspond to plasma depletions rather than plasma enhancements as the degree of depletion is an order of magnitude larger compared to the degree of enhancement with respect to the background ionization level during Spread F events. In addition to that, relatively small enhancements are often embedded in the depletion zones (see S7), making the identification by optical imaging technique even more difficult. However, using narrow band photometry with temperature-tuned interference filter, it is possible to unambiguously identify these structures in ESF.

As mentioned in Section 2, the radar observations were obtained at 14.8° N with respect to zenith. The optical measurements, on the other hand, correspond to the zenith direction. Therefore, it is clear that in spite of the radar and the optical instrument being collocated, two different spatial regions in the sky are probed by the radar and the photometer at the altitude range of 250–300 km. The regions probed by radar and the photometer are seperated along the meridional direction by 65–90 km. However, despite this horizontal seperation, a remarkable similarity between the radar structures and the micro variations in airglow intensity is observed. Tak-

[1]The region wherein the plasma enhancement is observed (see in Fig. 1), the background ionospheric layer movement (see h'F variation in Fig. 1C) is not downward. However, the velocities inside the structure is downward (see Fig. 1B). This indicates that the plasma structure denoted by S1 is not a "fossil" bubble.

ing into consideration of the magnetic field-aligned nature of ESF structures, the magnetic field geometry over the Indian zone, and the altitude extent of the airglow emission layers, it is easy to visualize that the field line mapping is responsible for the similarity between the optical and radar measurements. This suggests that the micro variations are the manifestation of large-scale magnetic field-aligned structures like plasma bubbles which provide a platform for the generation of meter scale size plume structures. Earlier co-ordinated measurements (Tsunoda and Towle, 1979) revealing collocated large-scale bubble with meter scale size irregularities, provide support for the present observation. Owing to narrow band and narrow beam photometry, the plasma bubble and enhancement structures register micro variation in this type of photometry. Thus, this kind of photometry provides the opportunity to obtain both micro variations due to plasma structures and macro variations due to background ionization.

Figure 1 suggests that the seed perturbation with more than one wavelength is required to give rise to a plume structure modulated over a bottomside wave-like structure. In this connection, the numerical simulation of F-region plasma structures with two long wavelength modes as initial perturbation is relevant. That simulation revealed the presence of plasma enhancements which move downward at an altitude beyond 350 km (Sekar et al., 2001). These relative enhancement structures are found to vary with relative amplitude, wavelength and phases of the two modes. The present observation of 777.4-nm airglow intensity enhancement which is due to the plasma enhancement provides an experimental verification of the earlier prediction (Sekar et al., 2001).

5 Conclusions

Narrow band photometric observations on 630.0-nm and 777.4-nm emission lines reveal micro variations during equatorial Spread F nights, in addition to the usual macro variations. Such micro variations are not observed on a non Spread F night, whereas macro variations are seen on both Spread F and non Spread F nights. In addition to the well-known anti-correlation between the base height of the F-region and the macro variations of thermospheric airglow intensity, the variation of the base height, on occasion, manifests as a bottomside wave-like structure. Using coordinated airglow and VHF radar measurements, the micro variations are identified to be due to the plasma structures associated with equatorial Spread F and found to be in correspondence with the VHF radar plume structures. Further, on some occasions, the VHF radar structures observed well beyond 350 km and moving downward are characterized as plasma enhancements. The observation of enhancement in 777.4-nm airglow intensity, which is characterized as plasma enhancement, brings out the importance of the multiple modes as seed perturbation in the generation of equatorial Spread F.

Acknowledgements. The authors thank the Director and the staff members of the National MST Radar Facility for their cooperation in making the observational campaign successful. This work is supported by the Department of Space, Government of India.

Topical Editor M. Lester thanks B. Reinisch and another referee for their help in evaluating this paper.

References

Barbier, D.: Recherches Sur la raie 6300 de la luminescence atmospherique nocturne, Ann. Geophysicae, 15, 179, 1959.

Haerendel, G.: Report - Theory of equatorial spread F, Max-Planck Inst. Fur Phys. and Astrophys., Garching, Germany, 1974.

Herrero, F. A. and Meriwether, J. W. Jr.: 6300A Airglow meridional intensity gradients, J. Geophys. Res., 85, 4191, 1980.

Huang, C. S. and Kelley, M. C.: Nonlinear evolution of equatorial spread F, 2. Gravity wave seeding of Rayleigh-Taylor instability, J. Geophys. Res., 101, 293, 1996.

Huba, J. D. and Ossakow, S. L.: On the generation of 3-m irregularities during equatorial spread F by low frequency drift waves, J. Geophys. Res., 84, 6697, 1979.

Kelley, M. C., LaBelle, J., Kudeki, E. et al.: The Condor equatorial spread F Campaign: Overview of results of the large-scale measurements, J. Geophys. Res., 91, 5487, 1986.

Kulkarni, P. V. and Rao, V. R.: 6300 A° night airglow emission over the magnetic equator, Ann. Geophys., 28, 475, 1972.

Laakso, H., Aggson, T. L., Pfaff, R. F., and Hanson, W. B.: Downdrafting plasma flow in equatorial bubbles, J. Geophys. Res., 99, 11 507, 1994.

Mendillo, M., Spence, H., and Zalesak, S. T.: Simulation studies of ionospheric airglow signatures of plasma depletions at the equator, J. Atmos. Terr. Phys., 47, 885, 1985.

Mendillo, M., Baumgardner, J., Colerico, M., and Nottingham, D.: Imaging Science Contribution to equatorial aeronomy: initial results from the MISETA Program: J. Atmos. Sol. Terr. Phys., 59, 1587, 1997.

Ossakow, S. L.: Spread F theories: A review: J. Atmos. Terr. Phys., 43, 437, 1981.

Patra, A. K., Ananadan, V. K., Rao, P. B., and Jain, A. R.: First observations of equatorial spread F from Indian MST radar, Radio Sci., 30, 1159, 1995.

Patra, A. K., Rao, P. B., Anandan, V. K., and Jain, A. R.: Radar observations of 2.8 m equatorial Spread F irregularities, J. Atmos. Sol. Terr. Phys., 59, 1633, 1997.

Raghavarao, R., Gupta, S. P., Sekar, R., Narayanan, R., Desai, J. N., Sridharan, R., Babu, V. V., and Sudhakar, V.: *In-situ* measurements of winds, electric fields and electron densities at the onset of equatorial Spread F, J. Atmos. Terr. Phys., 49, 485, 1987.

Rao, P. B., Jain, A. R., Kishore, P., Balmuralidhar, P., Damle, S. H., and Vishwanathan, G.: Indian MST radar, 1, System description and sample vector wind measurements in ST mode, Radio Sci., 30, 1125, 1995.

Rao, P. B., Patra, A. K., Chandrasekhar Sarma, T. V., Krishnamurthy, B. V. , Subbarao, K. S. V., and Hari, S. S.: Radar observation of updrafting and downdrafting plasma depletions associated with equatorial Spread F, Radio Sci., 32, 1215, 1997.

Sahai, Y., Aarons, J., Mendillo, M., Baumgardner, J., Bittencourt, J. A., and Takahashi, H.: OI 630.0-nm imaging observations of equatorial plasma depletions at 16°S latitude, J. Atmos. Terr. Phys., 56, 1461, 1994.

Sekar, R., Gurubaran, S., and Sridharan, R.: All sky imaging Fabry-Perot Spectrometer for optical investigation of the upper atmosphere, Indian J. of Radio and Space Phys., 22,197, 1993.

Sekar, R., Suhasini, R., and Raghavarao, R.: Effects of vertical winds and electric fields in the nonlinear evolution of equatorial spread F, J. Geophys. Res., 99, 2205, 1994.

Sekar, R, and Kelley, M. C.: On the combined effects of vertical shear and zonal electric field patterns on nonlinear equatorial spread F evolution, J. Geophys. Res., 103, 20 735, 1998.

Sekar, R., Kherani, E. A., Rao, P. B., and Patra, A. K.: Interaction of two long-wavelength modes in the nonlinear numerical simulation model of equatorial Spread F, J. Geophys. Res., 106, 24, 765, 2001.

Sinha, H. S. S., Misra, R. N., Chandra, H., Shikha Raizada, Dutt, N., and Vyas, G. D.: Multi-wavelength optical imaging of ionospheric plasma depletions, Indian J. Radio and Space Phys., 25, 44, 1996.

Sipler, D. P., Biondi, M. A. , and Hake, R. D. Jr.: Studies of the motion of equatorial 630.0-nm airglow depletions, Planet. Space Sci., 29, 1267, 1981.

Sridharan, R., Sekar, R., and Gurubaran, S.: Two-dimensional high-resolution imaging of the equatorial plasma fountain, J. Atmos. Terr. Phys., 55, 1661, 1993.

Sridharan, R., Chandra, H., Das, S. R. et al.: Ionization Hole campaign - a coordinated rocket and ground-based study at the onset of equatorial Spread F : First results, J. Atmos. Sol. Terr. Phys., 59, 2051, 1997.

Szuszezewicz, E. P., Tsunoda, R. T., Narcisi, R., and Holmes, J. C.: Coincident radar and rocket observations of equatorial spread F, Geophys. Res. Lett., 7, 537, 1980.

Takahashi, H., Sahai, Y., Clemesha, B. R., Simonich, D., Teixeira, N. R., Lobo, R. M., and Eras, A.: Equatorial mesospheric and F-region airglow emissions observed from 4° south, Planet. Space Sci., 37, 649, 1989.

Tsunoda, R. T.: Magnetic field-aligned characteristic of plasma bubbles in the night time equatorial ionosphere, J. Atmos. Terr. Phys., 42, 743, 1980.

Tsunoda, R. T. and Towle, D. M.: On the spatial relationship of 1-meter equatorial Spread F irregularities and depletions in total electron content, Geophys. Res. Lett.,6, 873, 1979.

Weber, E. J., Buchau, J., Eather, R. H., and Mende, S. B.: North-South aligned equatorial airglow depletions, J. Geophys. Res., 83, 712, 1978.

Woodman, R. F. and La Hoz, C.: Radar observations of F-region equatorial irregularities, J. Geophys. Res., 81, 5447, 1976.